

HST/WFC3 In-Orbit Grism Performance

H. Kuntschner^a and H. Bushouse^b, M. Kümmel^a, J. R. Walsh^a, J. MacKenty^b

^aSpace Telescope European Coordinating Facility, European Southern Observatory,
Karl-Schwarzschild-Str. 2, 85748 Garching, Germany;

^bSTScI, 3700 San Martin Drive, Baltimore, MD 21218, USA

ABSTRACT

The Hubble Space Telescope (HST) Wide Field Camera 3 (WFC3) is fitted with three gratings for slitless spectroscopy. In the UVIS channel there is one grating, G280, for the near-UV to visible range (200 - 400nm; 1.4nm/pix). The IR channel has two gratings: G102 for the shorter (800-1150nm; 2.45nm/pix) and G141 for the longer (1100-1700nm; 4.65nm/pix) NIR wavelengths. Using Servicing Mission Observatory Verification (SMOV) and Cycle 17 calibration data we have assessed the performance of the gratings. We have measured the field-dependent trace locations and dispersion solutions and determined the throughputs. The trace and wavelength solutions for the IR gratings were found to be linear functions, varying smoothly across the field of view. The UVIS grating exhibits a highly bent trace and significantly non-linear dispersion solutions. The maximum throughputs for the G102 and G141 gratings, including the telescope optics, are 41% at 1100 nm and 48% at 1450 nm, respectively. Limiting magnitudes at S/N=5 and a 1h exposure are $J_{AB}=22.6$ and $H_{AB}=22.9$ for the G102 and G141 gratings, respectively. The calibration results are published in the form of sensitivity and configuration files that can be used with our dedicated extraction software aXe to reduce WFC3 slitless data.

Keywords: SM4, Hubble Space Telescope (HST), Wide Field Camera 3 (WFC3), grating spectroscopy

1. INTRODUCTION

The Wide Field Camera 3 (WFC3) is fitted with three gratings for slitless spectroscopy. In the UVIS channel there is one grating, G280, for the near-UV to visible range (200 - 400nm). The NIR channel has two gratings, G102 and G141, for the shorter (800 - 1150nm) and longer NIR wavelengths (1100-1700nm), respectively.

There are several noteworthy areas where slitless spectroscopy differs from slit spectroscopy which we will briefly summarize. Because there is no slit, the spatial extent of the target determines the spectral resolution. In the case of non-stellar sources, it is the extent of the target in the direction of dispersion that limits the spectral resolution. The extraction height in cross-dispersion direction can be controlled by the extraction software and is usually adjusted to the object extent in the cross-dispersion direction. The dispersion of the gratings can be well characterized, but in order to set the wavelength zero-point, it is necessary to know the position of the target in the field-of-view (FoV). To this extent grating observations typically consist of a pair of a direct image and a grating image taken at the same sky location. A further complication of grating spectroscopy is the frequent mutual overlap of spectra in both the spatial direction and in dispersion direction, even across different spectral orders and at target distances of many hundred pixels. Fig. 1 presents a visual impression of grating spectra for point sources in the three WFC3 grating modes.

Prior to launch, calibrations of the trace and wavelength solutions as function of target position within the FoV and also throughput measurements were determined in three thermal vacuum (TV) ground calibration campaigns. The final pre-flight calibration results are summarized in Refs. 1, 2 and 3.

In order to ease the process of WFC3 grating data reduction a dedicated, semi-automatic spectral extraction software package, called aXe,⁴ is available to extract, flat-field, wavelength- and flux-calibrate spectra. The spectral trace and dispersion solutions are a function of source position within the field of view (see also Sec. 2.1 & 2.2). These 2-dimensional variations can be well characterized and the resulting reference and calibration files are used in the extraction software aXe.

Further author information: (Send correspondence to H. Kuntschner)
H. Kuntschner: E-mail: hkuntsch@eso.org, Telephone: +49 89 3200 6465

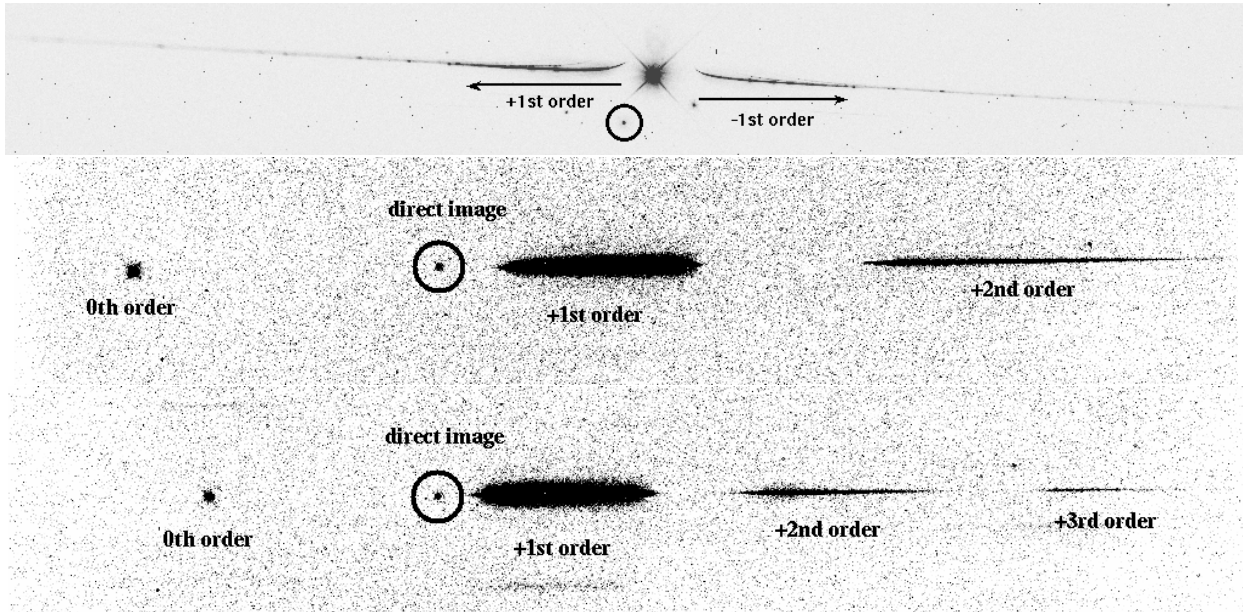


Figure 1. **Top:** Appearance of the UVIS G280 grism spectral orders on the detector. The circled source is the position of the direct image formed by summing an F300X image with the grism image. The stronger 1st order is to the left and the 0th order is in the center. Higher spectral orders are strongly overlapping and occupy the full extent of the detector. The image shows the full extent of the detector in the x-axis (4096 pixels) and about 500 pixels in the y-axis.

Middle: G102 grism observation of the flux standard star GD153 (program 11552) with a F098M direct image (circled) superimposed to illustrate the relative positions. Spectral orders 0, +1, and +2 can be seen on the image. The image shows the full extent of the detector in the x-axis (1014 pixels) and about 200 pixels in the y-axis.

Bottom: G141 grism observation of the flux standard star GD153 (program 11552) with a F140W direct image (circled) superimposed to illustrate the relative positions. Spectral orders 0, +1, +2, and +3 can be seen in the image. The image shows the full extent of the detector in the x-axis (1014 pixels) and about 200 pixels in the y-axis.

This report presents updated in-orbit calibrations for the grisms derived from SMOV and selected Cycle 17 calibration observations. An early analysis of the data was described in Refs. 5 and 6. Using data taken on WR stars, planetary nebulae and flux standard stars, we have assessed the performance of the grisms. We have measured the field-dependent trace locations and dispersion solutions and determined the throughputs for the near-IR grisms. All data shown in this report were processed with HST pipeline software `calwf3` version 2.0 and reference files available as of May 20, 2010.

2. THE NEAR-IR GRISMS

2.1 Trace calibration

In order to establish a good in-orbit trace (the location of the center of gravity in the spatial direction) calibration, we utilize the calibration observations of the wavelength standard planetary nebulae (PN) HB12. For the trace calibration, we are not interested in the primary target itself but in the other point sources around the primary target. This field (Galactic latitude: -02.85 degrees) comprises a relatively good compromise between field coverage and object density and thus avoiding too much spectral overlap between different sources in the FoV (see Fig. 2). The ST-ECF aXe software package for the reduction of slitless spectroscopy data treats the spectral traces and wavelength solutions as defined with respect to the position of the source in the direct image. The centroids of all sources above a given threshold in the F098M images (X_{ref} , Y_{ref}) were determined with SExtractor.⁷ These positions are assumed not to change between the observations of each direct image grism pair. The spectra of all sources were traced as a function of $\Delta X = X - X_{\text{ref}}$ in the detector X-direction by measuring the centroids of 7-10 pixel wide bins, using custom-written IDL programs. We found the traces of all orders (excluding the zeroth order) to be well fit by straight lines with standard deviations of 0.1 pixels. The

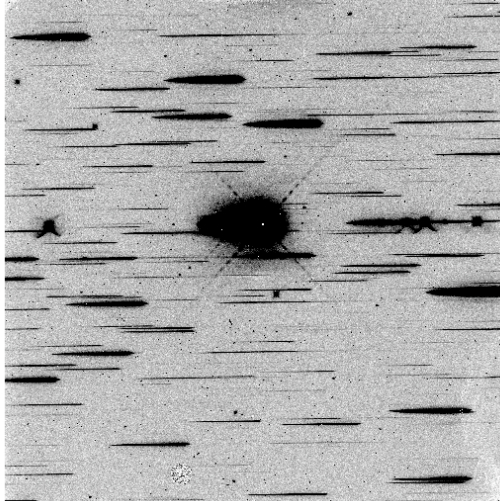


Figure 2. Image of a G102 grism exposure (iab907j6q.flt.fits). The primary target HB12 is located in the centre. Most of the other prominent spectra are first orders of different (stellar) objects in the FoV used for the trace calibration.

trace definitions are of the form $(Y - Y_{\text{ref}}) = \text{DYDX}_0 + \text{DYDX}_1 \cdot \Delta X$, where DYDX_0 and DYDX_1 are field dependent and given in the usual format used by the ST-ECF aXe reduction package, e.g., $\text{DYDX}_1 = a_0 + a_1 \cdot X_{\text{ref}} + a_2 \cdot Y_{\text{ref}} +$ (see also the aXe manual* for more details).

The final, field dependent trace solution for the $+1^{\text{st}}$ order of the near-IR grisms was derived from 137 (G102) and 162 (G141) different traces covering semi-uniformly the FoV. A graphical representation of the measured offsets and slopes for the G102 grism as a function of X_{ref} and Y_{ref} positions is given in Fig. 3. The offset shows a marked trend with Y_{ref} position while the slope shows a more complex dependence on X_{ref} and Y_{ref} . The offset is well represented with a field dependent fit using only a linear function (rms = 0.07 pixel), while the slope required a fit with quadratic terms (rms = 0.0004). The in-orbit calibrations show reasonably good agreement with the ground calibrations obtained in TV2 and TV3 with differences of ~ 0.3 pixel in the offset and good agreement for the slope.

For the -1^{st} , $+2^{\text{nd}}$ and $+3^{\text{rd}}$ orders, a similar procedure was carried out, however, due to the reduced field coverage for these orders the field dependent fits were more restricted and the trace prediction accuracy is reduced. For the 0^{th} order we adopt the trace determined in the ground calibrations. The same analysis was carried out for the G141 grism with similar results.

2.2 Wavelength solutions

In order to establish the in-orbit wavelength calibration, the PN Vy2-2 was observed as a wavelength calibrator as part of the Cycle 17 calibration program (Proposal 11937) over 9 different field positions.

For wavelength calibration one would ideally want point sources with clearly identifiable emission lines over the wavelength range and at the resolution of the grism. While bright, nearby PNs do show a reasonably good distribution of emission lines, they are slightly extended at the spatial resolution of the WFC3 IR camera. The PNs Vy2-2 and HB12 have already been used for HST/NICMOS grism calibrations⁸ and they offer a reasonable balance between brightness, number of emission lines and wavelength coverage, hence we opted for using those targets in the first wavelength calibrations of the WFC3 IR grisms.

For the G102 grism a total of nine emission features and for the G141 a total of seven emission features could be identified and used to establish the wavelength solution (see Tab. 1). Prior to determining the wavelength solution, the radial velocity of -71 km/s for Vy2-2 and an air to vacuum conversion was applied to the tabulated

*http://www.stecf.org/software/slitless_software/axe/

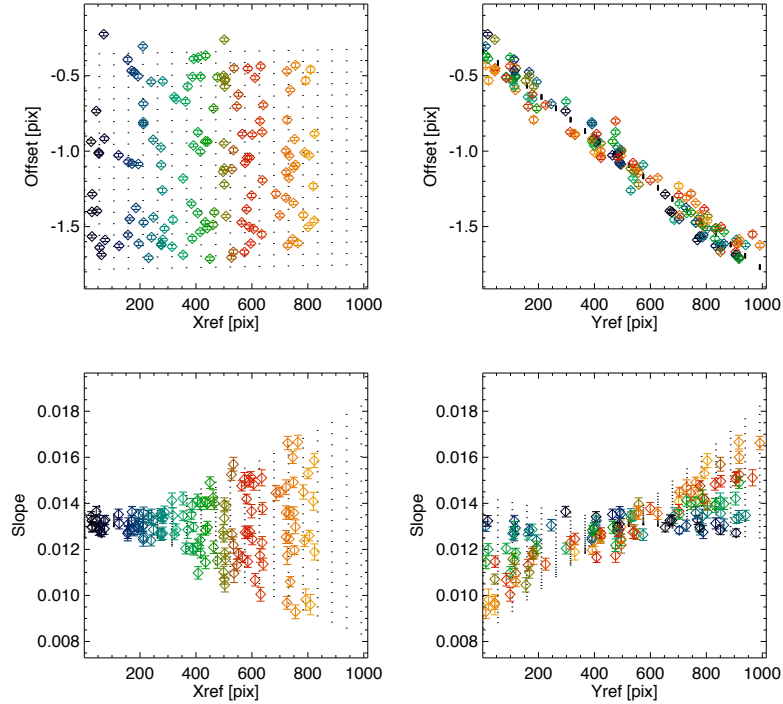


Figure 3. Example of trace fits for the G102 1st order spectra are shown as a function of X_{ref} and Y_{ref} position (colored diamond symbols). The top panels show the offset, while the bottom panels show the slope as function of X_{ref} and Y_{ref} . The color coding is linked to the X_{ref} position (see left panels). A total of 137 different source positions are used, covering well the field-of-view. The final field-dependent linear trace solution fit is shown as the grid of black dots.

wavelength of the emission lines. The ground calibration efforts suggested that a linear wavelength solution is a good representation of the true wavelength solution for these gratings.^{1,2} Therefore, we established for each spatial position a linear wavelength solution (see Fig. 4) where fits give a typical rms scatter of 0.2-0.3 pixel. The resulting wavelength solution for G102 shows typical errors of 5 Å for the zeropoint and 0.04 Å/pixel for the dispersion (~ 24.5 Å/pixel). For G141 the typical errors are 8 Å for the zeropoint and 0.06 Å/pixel for the dispersion (~ 46.5 Å/pixel).

Sometimes the emission lines are affected by e.g., cosmic ray hits, hot/dead pixels etc. and thus good emission line centroids could not be established. Therefore we used a 3-sigma rejection iteration for each linear fit to remove outliers. The He I line at 1083.03 nm is saturated in the data. However, we removed the saturated pixels from the fit and used the line wings to establish a fit to the line. There is marginal evidence in the in-orbit data for a non-linear wavelength solution, however, the deviations appear to be < 0.5 pixel over the full wavelength range. More wavelength calibration observations, including the use of true point sources (e.g., extra-galactic PN, Be stars), are needed to confirm any non-linear terms in the dispersion solution.

2.3 Throughput measurements

Using the trace and wavelength solutions described in the previous section, the spectra of the flux standard star GD153 observed in Proposal 11552 were extracted. Note, that we make use of our own "3D" flat-field calibrations for the G102 and G141 gratings, which significantly improve the quality of the spectra.^{5,6} There were four, slightly dithered, exposures for each of the near-IR gratings taken near the central position of the FoV. A further two exposures cover the top left and bottom right corners of the FoV. For the flux calibration we combine the +1st order of the four central exposures into a single spectrum with the help of the spectral drizzle option in the aXe software (aXedrizzle). This spectrum is used to establish the flux calibration for the near-IR

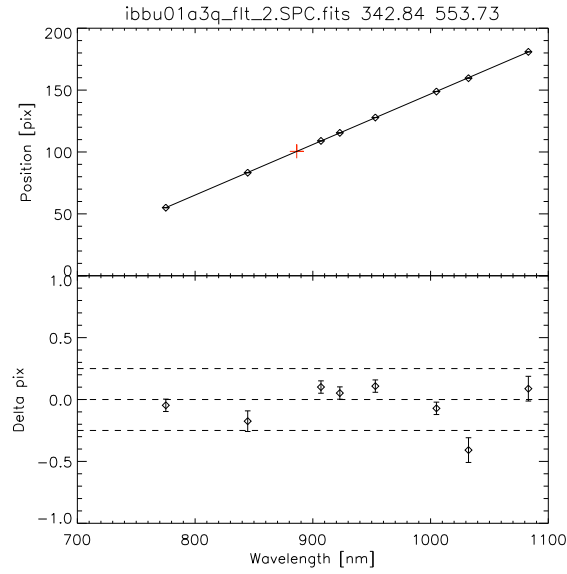


Figure 4. Linear fit for the wavelength solution of the G102 grism in the $+1^{st}$ order. The example shows a fit to one of the central pointings ($X_{ref} = 342.84$, $Y_{ref} = 553.73$). The top plot shows the fit whereas the bottom panel shows the deviations from the linear fit; the dashed lines indicate 0.25 pixel deviation from the fit.

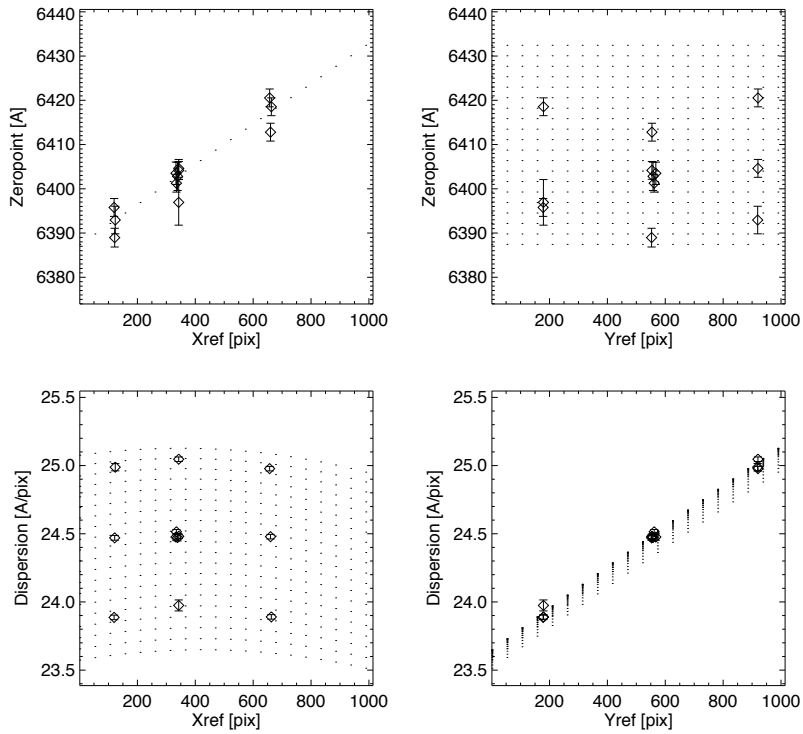


Figure 5. Example of the field dependent wavelength solution for the G102 1^{st} order spectra is shown as a function of X_{ref} and Y_{ref} position (diamond symbols). The final field-dependent wavelength solution is shown as the grid of black dots. The zeropoint shows a marked trend with X_{ref} whereas the slope is mostly dependent on Y_{ref} position.

Table 1. Rest air wavelength of emission features fitted to Vy2-2

Name	Wavelength (Å)
[Ar III]	7751.1
O I	8446.4
H P11	8862.8
[S III]	9068.6
H P9	9229.0
[S III]	9530.6
H P7	10049.4
[S II]	10321.9
He I	10830.3
He I	11969.1
He I	12784.9
H B13	16109.3
H B12	16407.2
H B11	16806.5
H B10	17362.1

Notes: Using a ground based spectrum⁹ of Vy2-2 the wavelengths used in the fits were adjusted: The rest wavelength of the [S II] emission line is 10328.9, however, the ground based spectrum suggests that at the spectral resolution of the G102 grism the effective peak wavelength is reduced by ~ 7 Å. For the G141 grism the ground based spectrum suggests that at the spectral resolution of the G141 grism the effective peak wavelength requires adjustments of -10.4 and +34.6 Å, for the He I emission lines at 11969.1 and 12784.9 Å.

grisms. The spectrum was converted to units of $[e^-/\text{Å}/\text{sec}]$ and divided by a smoothed version of the model spectrum taken from the HST CALSPEC library[†] (gd153_mod.007.fits). Median smoothing in a sliding 7 pixel window provides the final sensitivity function. The error is evaluated by taking the standard deviation of the four individual sensitivity curves from the central pointings at each wavelength bin and imposing a minimum error of 1%. Sensitivity curves were also derived for the 0th, +2nd, +3rd and -1st orders. While these orders are typically not used to extract science spectra, they are used in aXe to evaluate potential cross-contamination of other +1st order science spectra.

Fig. 6 shows the total instrument throughput including telescope and detector for the WFC3 near-IR grisms G102 and G141. The peak throughput for G102 is 41% at 1100 nm, while it is $> 10\%$ over the wavelength range 805 to 1150 nm. The G141 grism shows a peak throughput of 48% at 1450 nm while it is $> 10\%$ from 1080 to 1690 nm.

3. THE UV G280 GRISM

The analysis of the calibration observations for the UVIS G280 grism is still ongoing at the writing of this contribution. This grism was not re-designed for WFC3 but is a WF/PC1 spare. In contrast to the near-IR grisms there is an offset of about 175 pixels in the y-direction between the direct image and the spectra (see Fig.1), the zeroth-order is relatively bright (i.e. the star-like feature near the center of the G280 image in Fig.1) due to a lower grating efficiency and clear substrate, and there is significant curvature of the spectra at the blue ends of the first orders (nearest the zeroth order).

The amplitude of the curvature was determined from in orbit data of the wavelength calibration star WR14 observed as part of the Cycle 17 calibration program 11935. The amplitude is about 30 pixels in the detector y-direction (see Fig. 7)

[†]<http://www.stsci.edu/hst/observatory/cdbs/calspec.html>

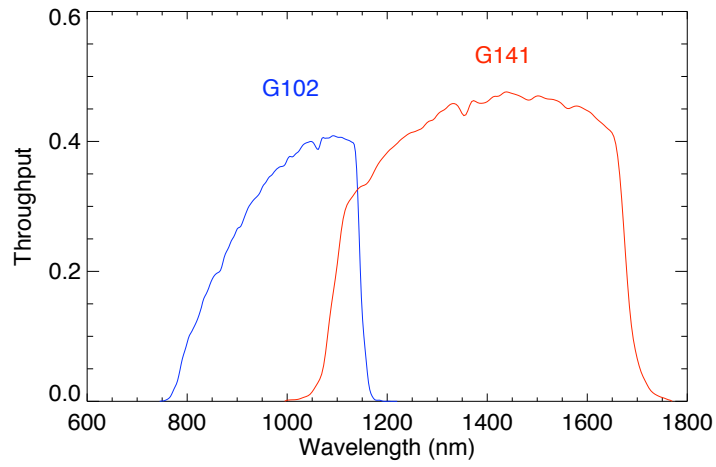


Figure 6. Total instrument throughput of the WFC3 near-IR grisms G102 (blue) and G141 (red).

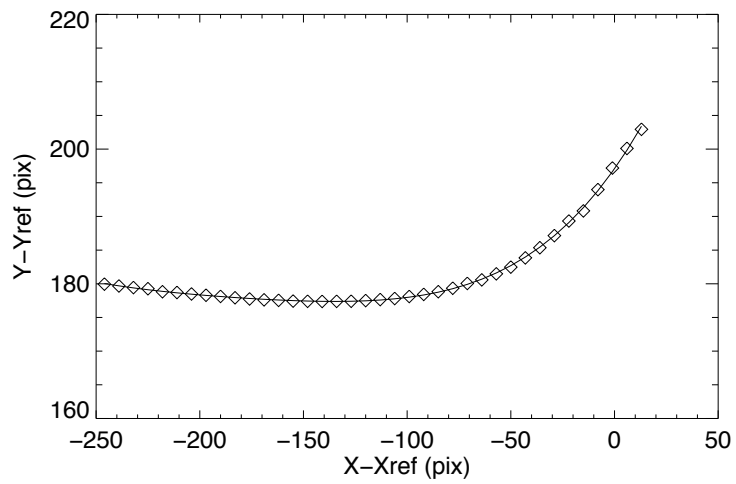


Figure 7. Trace of a UVIS G280 spectrum as function of $X-X_{\text{ref}}$ position on the detector. The observation used in this example is that of the wavelength calibration star WR14 (program 11935). Note the strong upturn towards increasing X-axis corresponding to lower wavelengths. The solid line shows a 5th order polynomial fit.

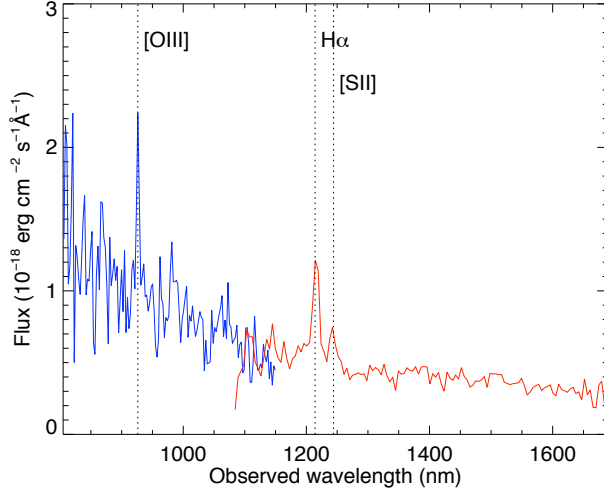


Figure 8. Example spectrum of a star-forming galaxy ($H_{AB} = 22.6$) at a redshift of $z = 0.85$ observed as part of the ERS grism observations.¹² The blue part of the spectrum was obtained with the G102 grism, while the red part of the spectrum was obtained with the G141 grism. Spectra are shown where the total throughput is above 10%; therefore there is a region of overlap at ~ 1100 nm.

4. FIRST SCIENCE RESULTS FROM THE NEAR-IR GRISMS

Current HST near-IR grism programs focus on studies to measure the evolution of cosmic star formation over the redshift range $z=0.3$ to 4. Refereed publications have recently been submitted to astronomical journals including first results from a dedicated HST parallel program (“The WFC3 Infrared Spectroscopic Parallel (WISP) Survey”;¹⁰ program 11696) and science derived from the WFC3 Early Release Science (ERS) program with grisms.^{11,12} All of these programs made already use of our dedicated data reduction software aXe and the associated calibration files. The combination of two near-IR grisms covering 800 to 1700 nm, often allows to detect and identify two or more emission lines which is crucial for secure redshift assignments. Namely, the $H\alpha$, [O III] and [O II] emission lines are visible in the WFC3 grisms at redshifts $0.2 < z < 1.6$, $1.2 < z < 2.4$ and $2.0 < z < 3.6$, respectively.

Fig. 8 shows an example spectrum extracted from the ERS data of a star-forming galaxy at a redshift of 0.85. Using the ERS grism data, we establish the limiting magnitudes at $S/N = 5$ per continuum pixel and for a 1h exposure to be $J_{AB} = 22.6$ and $H_{AB} = 22.9$ for the G102 and G141 grisms, respectively.

5. CONCLUSIONS

This report presented calibrations of the WFC3 grisms based on SMOV data and Cycle 17 calibration programs. We have established in-orbit, source position dependent calibrations of the trace and wavelength solutions for the near-IR grisms. Both, the local trace and wavelength solution can be approximated with a linear function. The mean dispersion of the G102 grism is $24.5 \text{ \AA}/\text{pixel}$ varying from 23.5 to $25.0 \text{ \AA}/\text{pixel}$ across the field of view. The mean dispersion of the G141 grism is $46.5 \text{ \AA}/\text{pixel}$ varying from 45.0 to $47.5 \text{ \AA}/\text{pixel}$ across the field of view. The trace and wavelength solutions for the UVIS G280 grism are currently under study.

For the near-IR grisms we establish flux calibrations for the $+1^{st}$ order. The total throughput of HST and the WFC3 G102 grism peaks at 1100 nm with 41% and is above 10% between 805 and 1080 nm. The G141 grism peaks at 1450 nm with 48% and is above 10% from 1080 to 1690 nm.

REFERENCES

- [1] Kuntschner, H., Bushouse, H., Walsh, J. R., and Kümmel, M., “The TV2 ground calibrations of the WFC3 NIR grisms,” tech. rep., ST-ECF Instrument Science Report WFC3-2008-15 (2008).

- [2] Kuntschner, H., Bushouse, H., Walsh, J. R., and Kümmel, M., “The TV3 ground calibrations of the WFC3 NIR grisms,” tech. rep., ST-ECF Instrument Science Report WFC3-2008-16 (2008).
- [3] Kuntschner, H., Bushouse, H., Kümmel, M., and Walsh, J. R., “The ground calibrations of the WFC3/UVIS G280 grism,” tech. rep., ST-ECF Instrument Science Report WFC3-2009-01 (2009).
- [4] Kümmel, M., Walsh, J. R., Pirzkal, N., Kuntschner, H., and Pasquali, A., “The Slitless Spectroscopy Data Extraction Software,” *PASP* **121**, 59–72 (2009).
- [5] Kuntschner, H., Bushouse, H., Kümmel, M., and Walsh, J. R., “WFC3 SMOV proposal 11552: Calibration of the G141 grism,” tech. rep., ST-ECF Instrument Science Report WFC3-2009-17 (2009).
- [6] Kuntschner, H., Bushouse, H., Kümmel, M., and Walsh, J. R., “WFC3 SMOV proposal 11552: Calibration of the G102 grism,” tech. rep., ST-ECF Instrument Science Report WFC3-2009-18 (2009).
- [7] Bertin, E. and Arnouts, S., “SExtractor: Software for source extraction.,” *A&AS* **117**, 393–404 (1996).
- [8] Pirzkal, N., Bohlin, R., and Thatte, D., “NICMOS Grism Wavelength Calibration,” tech. rep., STScI Instrument Science Report NICMOS-2009-006 (2009).
- [9] Hora, J. L., Latter, W. B., and Deutsch, L. K., “Investigating the Near-Infrared Properties of Planetary Nebulae. II. Medium-Resolution Spectra,” *APJS* **124**, 195–240 (1999).
- [10] Atek, H., Malkan, M., McCarthy, P., Teplitz, H., Scarlata, C., Siana, B., Henry, A., Colbert, J., Ross, N. R., Bridge, C., Bunker, A. J., Dressler, A., Fosbury, R. A. E., Martin, C., and Shim, H., “The WFC3 Infrared Spectroscopic Parallel (WISP) Survey,” *ArXiv e-prints*, 1005.4068 (2010).
- [11] van Dokkum, P. G. and Brammer, G., “Hubble Space Telescope WFC3 Grism Spectroscopy and Imaging of a Growing Compact Galaxy at $z=1.9$,” *ArXiv e-prints*, 1003.3446 (2010).
- [12] Straughn, A. N., Kuntschner, H., Kuemmel, M., Walsh, J. R., Cohen, S. H., Gardner, J. P., Windhorst, R. A., O’Connell, R. W., Pirzkal, N., Meurer, G., McCarthy, P. J., Hathi, N. P., Malhotra, S., Rhoads, J., Balick, B., Bond, H. E., Calzetti, D., Disney, M. J., Dopita, M. A., Frogel, J. A., Hall, D. N. B., Holtzman, J. A., Kimble, R. A., Luppino, G., Paresce, F., Saha, A., Silk, J. I., Trauger, J. T., Walker, A. R., Whitmore, B. C., and Young, E. T., “HST WFC3 Early Release Science: Emission-Line Galaxies from IR Grism Observations,” *ArXiv e-prints*, 1005.3071 (2010).